Journal of
Materials Chemistry B

Accepted Manuscript

This article can be cited before page numbers have been issued, to do this please use: I. J. Gomez, B. ARNAIZ, M. Cacioppo, F. Arcudi and M. Prato, *J. Mater. Chem. B*, 2018, DOI: 10.1039/C8TB01796D.

ROYAL SOCIETY OF CHEMISTRY

rsc.li/materials-b

View Article Online
DOI: 10.1039/C8TB01796D

Journal Name

ARTICLE

Nitrogen-doped Carbon Nanodots for bioimaging and delivery of paclitaxel

Received 00th January 20xx,
Accepted 00th January 20xx

DOI: 10.1039/x0xx00000x

www.rsc.org/

I. Jennifer Gomez,[a,b] Blanca Arnaiz,[a] Michele Cacioppo, [b] Francesca Arcudi [b] and Maurizio Prato*[a,b,c]

Carbon nanodots (CNDs) hold great potential in imaging and drug delivery applications. In this study, nitrogen-doped CNDs (NCNDs) were coupled to the anticancer agent paclitaxel (PTX) through a labile ester bond. NCNDs showed excellent cell viability and endowed the NCND-PTX conjugate with good water solubility. The hybrid integrates the optical properties of the nanodots with the anticancer function of the drug into a single unit. The cytotoxicity was evaluated in breast, cervix, lung, prostate cancer cell lines by the MTT assay while the cellular uptake was monitored using confocal microscopy. NCND-PTX induced apoptosis in cancer cells exhibiting slightly better anticancer activity compared to the drug alone. Moreover, the course of NCND-PTX interaction with cancer cells was monitored through the xCELLigence system. The NCND-based conjugate represents a promising platform for bioimaging and drug delivery.

1. Introduction

Carbon nanodots (CNDs) are quasi-spherical nanoparticles with size below 10 nm, which have recently gained great popularity as novel luminescent materials.[1,2] CNDs possess many favorable properties, including easily available and non expensive precursors, facile and low cost production, high photostability, biocompatibility, tuneable emission and good solubility in a variety of solvents.[3,4] These features make CNDs a promising alternative to heavy metal-based quantum dots, useful for application in a wide range of technologies, including sensing, biomedical and optoelectronic applications.[5–8]
Moreover, engineering the CND surface and exploiting the reactivity of functional groups for covalent or supramolecular interactions with functional molecules is a key to tune their properties and meet the requirements for specific tasks.[9–19] The synergistic integration of the component functionalities should enable the construction of nano-assemblies with superior and unique properties.[20–26] Considering the low toxicity nature, CNDs have opened new possibilities for biomedical purposes.[27,28] CNDs can be readily internalized by different types of cells: several research groups have evaluated their potential as bioimaging agents in cellular or *in vivo* environments.[28–30] Moreover, CNDs have emerged as a versatile platform for the design of novel drug delivery systems with promising studies reporting the use of CNDs as nanocarriers for the delivery of therapeutic agents,[31–33] such as doxorubicin.[34–36] CNDs retain their luminescence after the loading of the drugs, either through electrostatic interaction or covalent binding, serving not only as a vehicle for drug delivery, but also for cell imaging. Despite many achievements, a simple and effective preparation of CNDs capable of further modifications to be included in a stable and multifunctional water carrier for hydrophobic drugs, remains a challenge. Most anticancer drugs have hydrophobic nature and unlocking their full therapeutic potential requires drug formulation strategies. Among these, Paclitaxel (PTX) is one of the most effective cancer therapeutics to treat diverse solid tumors,[37,38] and can be considered as a test case for any delivery system because of its poor solubility in water. It is commonly formulated as "Taxol", which include a combination of Cremophor EL and ethanol for solubilization. However, severe hypersensitivity reactions and side effects associated with this excipient or adjuvant have been found.[39,40] Numerous attempts are being made to increase the solubility and the pharmacokinetic profile of the PTX using alternative formulations, including liposomes, micelles, prodrug strategies or nanoparticles.[41–43] Especially the latter have attracted increasing attention with various nanoparticle delivery systems, including polymeric or inorganic nanoparticles, that have been studied for several decades, while alternative systems continue to rapidly gain interest.[41,42]

[a] Carbon Nanobiotechnology Laboratory, CIC biomaGUNE, Paseo de Miramón 182, 20014 Donostia-San Sebastián, Spain
[b] Department of Chemical and Pharmaceutical Sciences, INSTM UdR Trieste, Via Licio Giorgieri 1, University of Trieste, 34127 Trieste, Italy.
[c] Basque Foundation for Science, Ikerbasque, 48013 Bilbao, Spain.
*Email: prato@units.it

Electronic Supplementary Information (ESI) available: [details of any supplementary information available should be included here]. See DOI: 10.1039/x0xx00000x

Here, we report a CND-based drug nanocarrier, based on a facile, fast and cost-effective microwave-assisted method to prepare fluorescent, water soluble and biocompatible nitrogen-doped CNDs (NCNDs) that allow an efficient covalent binding of drugs on their surface. In order to showcase the features of this platform in cancer therapy, the basically water insoluble PTX was chosen in this study as a model drug. The cellular uptake and *in vitro* cytotoxicity of the conjugate was evaluated against various cell lines and compared with the drug alone. Dynamic data about the global cell proliferation were obtained from a real-time cell analysis system by employing the xCELLigence technology. Finally, a drug-release study is presented and the effect of the conjugate on cell apoptosis was investigated using confocal fluorescence microscopy.

2. Experimental details

2.1 Materials

L-Arginine (≥98%), ethylenediamine (≥99.5%), paclitaxel (≥97%), *N*-(3-dimethylaminopropyl)-*N'*-ethylcarbodiimide hydrochloride (EDC) (≥98%), *N*-hydroxysuccinimide (≥98%), succinic anhydride (≥99%), *N,N*-dimethylformamide (≥99.8%), pyridine (≥99%), kaiser test kit and Sephadex LH-20 were purchased from Sigma-Aldrich. Cyanine 5-NHS ester was purchased from Lumiprobe. Ultrapure fresh water obtained from a Millipore water purification system (>18MΩ Milli-Q, Millipore) was used in all experiments. PBS solution (pH 7.4) was prepared using Milli-Q water and PBS tablets purchased from Sigma Aldrich. All chemicals were used without further purification. Dialysis membrane tubes (0.5-1 kDa) were bought from Spectrum Labs. All cell lines were purchased from ATCC-LGC and cultured in DMEM or RPMI-1640 media from Sigma Aldrich completed with 2 nM L-glutamine, 100 u·mL^{-1} penicillin, 100 ug·mL^{-1} streptomycin and 10% heat-inactivated fetal bovine serum from Gibco®. Cell proliferation kit I was purchased from Roche and was used to quantify relative cell viability (3(4,5-dimethylthiazol-2-yl)-2,5-diphenyltetrazolium bromide, MTT).

2.2 Apparatus and Methods

The microwave synthesis was performed on a CEM Discover-SP. NMR experiments were carried out with a Varian Inova (500 MHz) in DMSO-d_6 using the solvent residual peak as internal reference. The self-diffusion coefficient evaluations were carried out using Varian Inova (500 MHz) NMR spectrometer equipped with Performa II-Z gradient coils (Varian, Palo Alto, CA, USA) using diffusion gradient length = 4.0 msec and diffusion delay = 75.0 msec. UV-Vis spectra were recorded on a Jasco V-630 Bio spectrophotometer. Fluorescence spectra were recorded on a Perkin Elmer LS55 fluorimeter. All the spectra were recorded at room temperature using 10 mm path-length cuvettes. Fourier-transform infrared spectra (KBr) were recorded on a ThermoScientific Nicolet 6700 spectrometer. MALDI-TOF mass analyses were performed on an UltrafleXtreme III spectrometer equipped with a pulsed Nd:YAG laser (355 nm) and controlled by FlexControl 3.3 and FlexImaging 2.1 softwares (Bruker Daltonics, Germany). Atomic force microscopy (AFM) images were obtained with a Nanoscope IIIa, VEECO Instruments. As a general procedure to perform AFM analyses, tapping mode with a HQ:NSC19/ALBS probe (80 kHz; 0.6 N/m) (MikroMasch) from drop cast of samples in an aqueous solution (concentration of few mg/mL) on a mica substrate was performed. The obtained images were analyzed in Gwyddion 2.47. Absorbance of MTT product was detected in a micro plate reader GENios Pro, TECAN. The normalized cell index in real time was measured on a xCELLigence Real-Time Cell Analysis (RTCA). Fluorescence images were taken in a confocal microscope (Zeiss LSM 510 Meta) with laser 488 nm, 505 LP filter and 20X magnification objective with differential interference contrast for transmitted light.

2.3 Syntheses

2'-Succinyl-paclitaxel

2'-Succinyl-paclitaxel was prepared according to a previously reported synthetic protocol.[44] A solution of 100.0 mg (0.1 mmol) of paclitaxel and 152.0 mg (1.5 mmol) of succinic anhydride in 2.4 mL of pyridine was stirred at r.t. for 3 h. The mixture was evaporated to dryness in vacuo and the residue was treated with 20.0 mL of water, stirred for 20 min, and filtered. The precipitate was dissolved in acetone, water was slowly added, and the white crystals were collected (67.0 mg, 59% yield).^{1}H NMR (DMSO-d_6) δ: 12.26 (s, 1H), 9.21 (d, J = 8.5 Hz, 1H), 7.97 (d, J = 8.5 Hz, 2H), 7.84 (d, J = 8.5 Hz, 2H), 7.73 (t, J = 7.4 Hz, 1H), 7.69 – 7.62 (m, 2H), 7.59 – 7.42 (m, 6H), 7.19 (ddd, J = 8.7, 5.7, 3.2 Hz, 1H), 6.29 (s, 1H), 5.81 (t, J = 8.8 Hz, 1H), 5.53 (t, J = 8.7 Hz, 1H), 5.40 (d, J = 7.2 Hz, 1H), 5.35 (d, J = 8.9 Hz, 1H), 4.90 (d, J = 7.1 Hz, 2H), 4.62 (s, 1H), 4.10 (dt, J = 11.0, 6.9 Hz, 1H), 4.00 (dd, J = 16.1, 8.3 Hz, 2H), 3.57 (d, J = 7.2 Hz, 1H), 2.66 – 2.57 (m, 3H), 2.43 – 2.28 (m, 3H), 2.23 (s, 3H), 2.10 (s, 3H), 1.81 (dd, J = 15.0, 9.2 Hz, 2H), 1.75 (s, 1H), 1.69 (s, 1H), 1.63 (dd, J = 14.7, 10.8 Hz, 2H), 1.49 (s, 3H), 1.00 (d, J = 13.5 Hz, 6H). MS (IE$^+$), *m/z*: 953.3 (M$^+$).

NCNDs

NCNDs were synthesized according to our previously reported method,[45] through microwave irradiation of an aqueous solution of L-Arginine (Arg) and ethylenendiamine (EDA). 87.0 mg (0.5 mmol) of L-Arginine, 33.0 µL (0.5 mmol) of EDA and 100 µL of Milli-Q water were heated at 240 °C, 26 bar and 200 W for 180 seconds. In the process of microwave heating, the solution changes color from transparent to brown as a result of formation of NCNDs. The solution was diluted with water and was filtered through a 0.1 µm microporous membrane separating a deep yellow solution that was dialyzed against pure water through a dialysis membrane for 2 days. The aqueous solution of NCNDs was lyophilized giving 27.0 mg of a brownish solid.

NCND-PTX

The hybrid material was prepared according to slightly modified literature procedures.[12,13] To a solution of 100.0 mg (0.1 mmol) of 2'-succinyl-paclitaxel in 5.0 mL of anhydrous

View Article Online
DOI: 10.1039/C8TB01796B

DMF, 30.0 mg (0.2 mmol) of EDC and 18.0 mg (0.2 mmol) of NHS were added. The mixture was stirred at 0 °C for 1 h. 40.0 mg of NCNDs were added and the resulting mixture was stirred at r.t. overnight. The solvent was removed under reduced pressure and the crude mixture was dissolved in MeOH and isolated by size exclusion chromatography using a column packed with Sephadex LH20 (eluting with MeOH). Finally, the solvent was removed under reduced pressure obtaining 90.0 mg of NCND-PTX as a yellow solid.

NCND-Cy5

A solution of 40.0 mg of NCNDs and 2.5 mg of cyanine 5-NHS ester in 5.0 mL of anhydrous DMF was stirred at r.t. overnight. The solvent was removed under reduced pressure. The crude mixture was diluted with water and was filtered through a 0.1 µm microporous membrane separating a blue solution that was dialyzed against pure water through a dialysis membrane for 1 day. The aqueous solution of NCND-Cy5 was lyophilized giving 38.0 mg as a blue solid.

NCND-PTX-Cy5

A solution of 50.0 mg of NCND-PTX and 2.5 mg of cyanine 5-NHS ester in 5.0 mL of anhydrous DMF was stirred at r.t. overnight. The solvent was removed under reduced pressure. The crude mixture was diluted with water and was filtered through a 0.1 µm microporous membrane separating a blue solution that was dialyzed against pure water through a dialysis membrane for 1 day. The aqueous solution of NCND-PTX-Cy5 was lyophilized giving 14.0 mg as a blue solid.

2.4 Stability studies

NCNDs were incubated at 37 °C in a humidified atmosphere with 5% CO_2, under the following conditions: Dulbecco's modified Eagle's medium (DMEM) medium completed with 10% heat-inactivated fetal calf serum (FBS), 2.0 mM L-glutamine(Gibco), 100.0 U·mL^{-1} penicillin and 100.0 µg·mL^{-1} streptomycin (Gibco). The absorbance of the dots was monitored at 24 h, 48 h and 72 h.

2.5 Cell culture and counting

All the cell lines used in this study were cultured in complete Dulbecco's Modified Eagle's Medium (DMEM) and Roswell Park Memorial Institute medium (RPMI) at 37 °C in humidified atmosphere of 5 % CO_2 in tissue culture-treated 75 cm^2-flasks (from Nunc). For cell passage, adherent cells were lifted from the flasks by incubation at 37 °C with trypsin-EDTA solution 1x (2.5 g porcine trypsin and 0.2 g EDTA • 4 Na per liter of Hanks' Balanced Salt from Sigma), span at 1000 g for 5 min and the pellet re-suspended in 1 ml media. For cell counting, the cell suspension was serially diluted 1:10 in PBS and 1:2 in the exclusion dye Trypan Blue solution (0.4 % in 0.8 % sodium chloride and 0.1 % potassium phosphate, dibasic from Sigma Aldrich), 10.0 µL of the diluted cell suspension was counted in a haemocytometer chamber under transmitted light in an inverted microscope (DMIL, Leica).

2.6 Cell viability assay

Cell viability of adherent human cell lines was measured with the colorimetric MTT assay. 4x10^3 PC3 (prostate cancer), 4x10^3 A-549 (small cell lung carcinoma), 2.5x10^3 C33-A (cervix carcinoma), 2.5x10^3 HeLa (cervix carcinoma), 4x10^3 MDA-MB-231 (breast adenocarcinoma), 10x10^3 MCF-7 (breast adenocarcinoma) cells were seeded in a 96 well plates (200 µL media per well) and cultured for 24 h at 37 °C and 5% CO_2. Then, they were incubated (at 37 °C in a humidified atmosphere with 5% CO_2 for 72 h) in 100 µL of medium containing different concentrations of NCND-PTX. The cells were then washed twice with 100.0 µL of incomplete medium and incubated and 5 % CO_2 with 100.0 µL media containing MTT at the (1:20 dilution) at 37 °C for 30-60 min. The MTT-formazan was dissolved in 100.0 µL of DMSO and the absorbance was measured in a micro plate reader (Genios Pro, TECAN) at 550 nm. Data are expressed as a percentage of absorbance of treated cells related to the untreated control cells and represented as means of quadruplicates ± SD.

2.7 Statistical analyses

Comparison of two-variable data were performed using two-way ANOVA with Bonferroni adjustment. A p value < 0.05 was accepted as statistically significant (GraphPad Prism, GraphPad Software, La Jolla, CA).

2.8 Real-time Cell Electronic Sensing (RT-CES) and Cell Index (CI) measurements

Experiments for time-dependent cell response were carried out accordingly to previously described procedures.[46] 100.0 µL of media was added to 16 well-electronic plates (E-Plates). Following the background readings, 100.0 µl of cell suspension was added and the E-Plates were incubated at room temperature for 30 min and then, inserted on the reader, which was placed in a humidified incubator at 37 °C and 5% CO_2 for continuous recording of impedance as reflected by the cell index. All the measurements by the RT-CES were performed inside an incubator at 37 °C, 5% CO_2 and humidified atmosphere. After 24 h the cells were treated with different concentrations of NCND-PTX. The impedance was recorded every five minutes for the duration of 8 h to capture the short-term response, followed by measurements every 30 min for 72 h and every 15 min for 24 h in order to capture the long-term response. The Cell Index (CI) was derived according to the following equation:

$$\mathrm{CI}= \max_{i=1,\ldots,N}\left(\frac{R_{cell}(f_i)}{R_b(f_i)}-1\right)$$

where $R_{cell}(f)$ and $R_b(f)$ are the frequency-dependent electrode resistances with or without cells, respectively, and N is the number of the frequency points at which the impedance is measured. The Normalized Cell Index at a given time point was calculated by dividing the Cell Index at the time point by the Cell Index at a reference time point.

2.9 Fluorescence microscopy

View Article Online
DOI: 10.1039/C8TB01796D

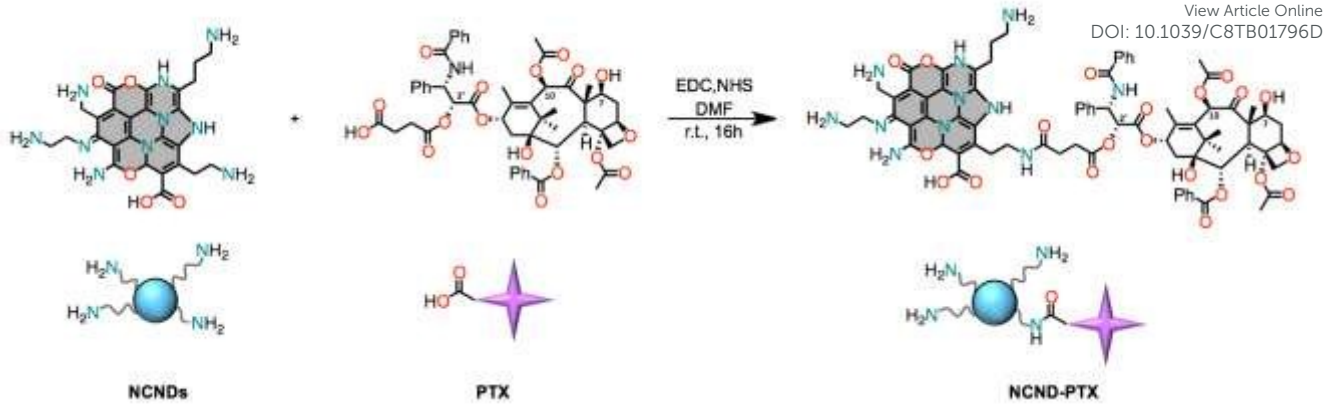

Figure 1. Synthetic scheme for the covalently linked nitrogen-doped CNDs (a representative structural unit is depicted)-paclitaxel (NCND-PTX) used in this study.

$4x10^3$ C33-A, $4.5x10^4$ PC-3, $4.5x10^4$ A-549, $3.5x10^4$ HeLa, $1.4x10^5$ MCF-7 and $4.5x10^4$ MDA-MB-231 cells per well were seeded onto sterile 13 mm round cover glasses in a 48 well plate (Millicell EZslide, Millipore) and cultured for 3 days. Supernatants were replaced by 250.0 µL media alone or media containing NCNDs (300.0 $\mu g \cdot ml^{-1}$), then incubated for 24 h at 37 °C and 5% CO_2. The cells were washed twice with sterile PBS prior to fixation with sterile PBS containing 4% paraformaldehyde for 15 min at room temperature. Wells were disassembled, cells were washed twice with PBS and, the slide was mounted with 1 drop mounting media (DAKO) and a 1.5 coverslip (24x60mm). For morphological studies of apoptosis, $5x10^3$ A-549 cells per well were seeded onto sterile 1.5 coverslips in a 48 well plate, cultured for 3 days and incubated with media alone or media containing 20 $ng \cdot ml^{-1}$ of NCND-PTX-Cy5, or NCND-Cy5 for 24 h at 37 °C and 5% CO_2. Cells were washed and fixed as described above. After PBS washing, the cells were treated with 125.0 $ng \cdot mL^{-1}$ DAPI (4',6-diamidino-2-phenylindole) in PBS at r.t. for 10 min. Cells were washed again and the round coverslip was mounted onto a slide with 1 drop mounting media (DAKO). The mounted slides were let to harden overnight at 4°C. Images were taken in a confocal microscope (LSM 500 meta, Zeiss), plan-Apochromat 63x/1.40 Oil DIC M27 objective and with laser 405 nm/BP 420-605 nm filter, or laser 633 nm/BP 650-755 filter.

2.10 *In vitro* drug release

The THP-1 cells were seeded in 24 well plates ($1.6x10^6$ cells per well) and cultured for 24 h at 37 °C and 5% CO_2. The medium was replaced with NCND-PTX (1 $mg \cdot mL^{-1}$). After incubation (24 h), the cells were washed twice and re-suspended in PBS. Then the cell suspensions were lysed by three freeze/unfreeze cycles in liquid nitrogen followed by 15 min of sonication. The resulted lysate was passed through a centrifuge 3 kDa (Amicon) filter, and the collected fraction was analysed by fluorescence spectroscopy. Untreated cells served as control.

3. Results and discussion

3.1 Preparation and characterization of NCND-PTX

CNDs can be made from a variety of organic compounds or carbonaceous materials by either top-down or bottom-up routes.[3,4,29] We built on our previously reported simple and cost-effective bottom-up approach using a microwave reactor under controlled conditions.[45] Arginine and ethylenediamine have been used as carbon and nitrogen precursors for nitrogen-doped CNDs (NCNDs). They display a quasi-spherical shape and various oxygen and nitrogen functional groups on the surface. Moreover, NCNDs show the typical excitation wavelength dependent emission behaviour. Herein we want to take advantage of their fluorescence, high solubility in water and the presence of amines on their surface, which have shown to be reactive for covalent functionalization,[12,13] in order to prepare a fluorescent and water soluble NCND-based drug nanocarrier. The advantage of forming a conjugate with enhanced aqueous solubility would increase the bioavailability of the drug and therefore have a potential to enhance its activity. Beside solubility, the bioavailability depends on the bond between the drug and the carrier since specific spacers favor the drug release from the conjugate.

PTX was selected as the model water-insoluble anticancer drug in our study. Usually the hydroxyl C2' site is more reactive than the C7 site due to less hindrance.[47]

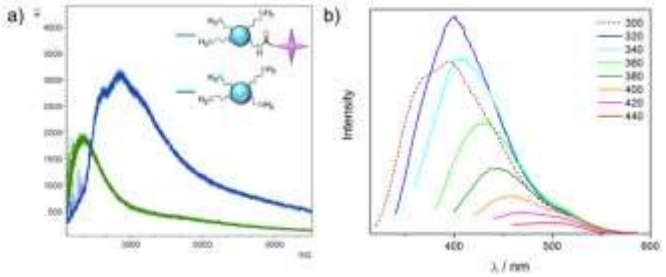

Figure 2. a) MALDI of the NCND-PTX conjugate and NCND reference; **b)** FL spectra of NCND-PTX in water (25 °C) at different excitation wavelengths.

View Article Online
DOI: 10.1039/C8TB01796D

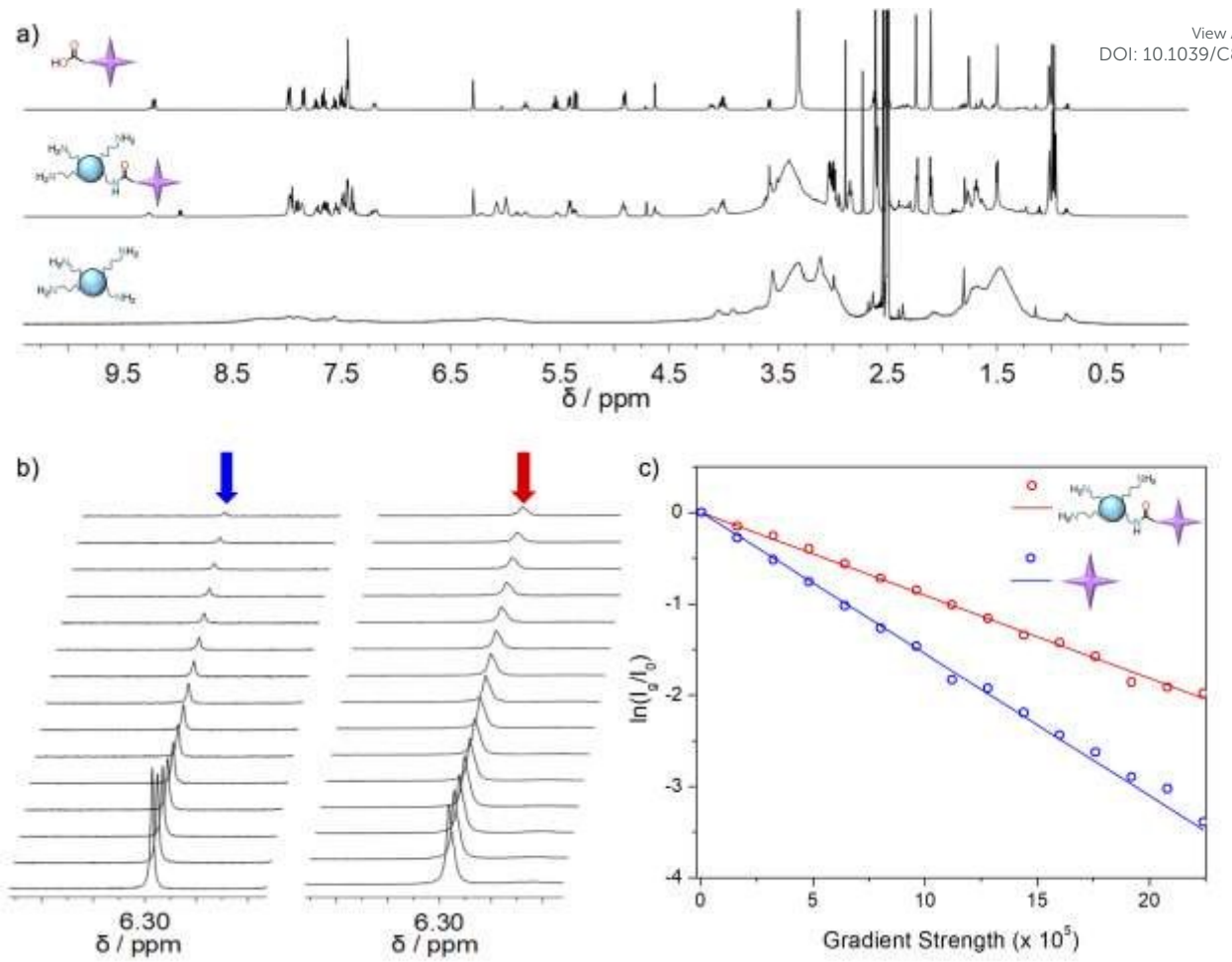

Figure 3. a) ^{1}H-NMR (DMSO-d_6, 298 K, 500 MHz) of 2'-succinyl- paclitaxel (top), NCND-PTX (center) and NCNDs (bottom); **b)** DOSY (DMSO-d_6, 298 K, 500 MHz) stack plot showing the signal decay in PTX (left) and NCND-PTX (right) of representative peak (H-10 singlet, 6.29 ppm) as function of gradient strength; **c)** Normalized logarithmic signal decays versus the diffusion weighing of representative peaks of PTX (blue) and NCND-PTX (red) with the corresponding linear fits.

On the basis of the above rationale, it was reasoned that the most feasible route for the preparation of the hybrid was to react the amino groups of the dots with a 2'-activated paclitaxel derivative. We used succinic anhydride as spacer to bind PTX to the dots. Therefore, PTX was first reacted with succinic anhydride at the 2'-hydroxyl position forming an ester bond and introducing a free carboxyl acid group. As depicted in **Figure 1**, the drug was covalently attached to the amino groups on the NCND surface via a carbodiimide condensation reaction (see Experimental for details). The conjugate was purified by size exclusion chromatography and was found to be soluble in water. In the present conjugation reaction, the formation of an ester bond provides a site for hydrolysis to release the free drug after internalization of the hybrid into the cancer cell.[48,49]

Matrix-assisted laser desorption ionization (MALDI) was employed to measure the molecular mass of the NCND-PTX conjugate, which was larger than that of NCNDs confirming the successful covalent linkage between PTX and NCNDs (**Figure 2a**): 3 kDa and 1 kDa for the NCND-PTX and the NCNDs, respectively, have been found, indicating that the conjugate has ca 2 drug molecules per dot, as determined by the mass difference between the conjugate and the parent dots (blue and green line, respectively). On the other hand, kaiser test was used to estimate the amount of free amino groups on the dot surface after the covalent coupling of the drug. The noticeable decrease of the amount of amines in the NCND-PTX (130 μmol·g^{-1}) as compared to the NCNDs (1350 μmol·g^{-1})[45] confirmed the functionalization reaction.

The size and morphology of the as-prepared NCND-PTX was characterized by atomic force microscopy. NCNDs are spherical nanoparticles with an average size of around 2.5 nm,[45] and an increased size of around 8 nm after the conjugation with PTX, in agreement with MALDI experiments, was observed (**Figure S1**). The chemical structure was characterized using ^{1}H-NMR and FTIR spectroscopies. ^{1}H-NMR investigation supported the successful functionalization of the NCNDs surface with PTX. The ^{1}H-NMR spectrum of NCND-PTX showed both the signals expected for NCNDs and PTX. The disappearance of the signal related to the carboxylic acid (at 12.26 ppm) of the 2'-succinyl-paclitaxel as well as the appearance of amide NH (at 9.25 ppm) in the conjugate suggests the hybrid formation (**Figures 3** and **S2**). Almost all the signals from the conjugate are broader as compared to those of the free drug because of the decreased rotational mobility when covalently attached to the nanoparticle.[50] Finally, diffusion ordered spectroscopy (DOSY)

View Article Online
DOI: 10.1039/C8TB01706D

Table 1. IC_{50} of the NCND-PTX conjugate and free PTX in MCF-7, MDA-MB-231, A-549, PC-3, C33-A and HeLa cell lines.

	NCND-PTX	free PTX
IC_{50} (ng·mL^{-1}) in MCF-7 cells	69.2	81.4
IC_{50} (ng·mL^{-1}) in MDA-MB-231 cells	65.1	91.0
IC_{50} (ng·mL^{-1}) in A-549 cells	30.4	34.6
IC_{50} (ng·mL^{-1}) in PC-3 cells	140.8	179.7
IC_{50} (ng·mL^{-1}) in C33-A cells	930.0	2820.0
IC_{50} (ng·mL^{-1}) in HeLa cells	3.4	2.9

was employed for the calculation of the diffusion coefficients for the free drug (D = 1.55 × 10^{-6} cm^2 s^{-1}) and the hybrid (D = 9.06 × 10^{-7} cm^2 s^{-1}). The smaller value obtained for the latter is in agreement with the formation of a higher-molecular weight species.[51,52]

Moreover, the FT-IR spectrum of the NCND-PTX showed the characteristic infrared signals of both NCNDs and PTX (**Figure S3**). The optical properties of the conjugate were investigated with UV-Vis and fluorescence (FL) spectroscopies. A slight shift of the absorption band at 286 nm, related to the π-π* transition of the C=C units of NCNDs, was observed as a consequence of the presence of the drug absorbing in the same spectral region (**Figure S5**). Accordingly, the emission profile suggested a surface modification of the dots after the coupling with drug. NCNDs showed the typical excitation-dependent FL that may arise from the presence of a distribution of emissive domains and fluorophores on their surface.[53–55] The NCND emission peak shifts from 356 nm to 474 nm when excited from 300 nm to 420 nm.[45] The coupling of the drug did not affect the emission properties of the dots (**Figure 2b**). However, a change in the optimal excitation wavelength (from 300 nm for the dots to 320 nm for the conjugate) was observed and suggest a different distribution of emissive sites on each dot after the functionalization. Taken together, these data confirm the successful conjugation of the drug on the surface of the nanodot.

3.2 Media stability, cell viability and imaging of NCNDs

To exploit NCNDs in biological applications, their stability in biological media and cell viability are two fundamental prerequisites that need to be satisfied. The stability of NCNDs was investigated at 37 °C and 5% CO_2 in cell culture dulbecco's modified eagle medium (DMEM) completed with 10 % heat-inactivated fetal bovine serum (FBS) through UV-Vis spectroscopy.[56] The solution was tested for 72 h and the dots were stable in cell culture media at all the different time intervals analyzed (0 h, 24 h, 48 h and 72 h; **Figure S6**).

On the other hand, the NCND biocompatibility was tested in cervix (C33-A, HeLa), breast (MCF-7, MDA-MB-231), lung (A-549) and prostate (PC-3) cancer cells by MTT colorimetric assay. The viability of the cell lines varies between 80-100 % after 72 h of incubation, with NCNDs in the concentration range of 1 μg·mL^{-1}- 1 mg·mL^{-1} (**Figure S12**), suggesting that the dots had no adverse effect on tumour cells, even at relatively high concentration.

Furthermore, the use of NCNDs as bioimaging probe was investigated by using confocal microscopy (**Figure 4** and **Figure S11**). Following 24 h of incubation, NCNDs could easily get internalized into the cells, which exhibit bright green fluorescence.

3.3 In vitro anti-tumoral activity of NCND-PTX

The *in vitro* cytotoxicity of NCND-PTX was investigated and compared with PTX by cell viability experiments. We evaluated the anticancer efficiency of NCND-PTX in breast (MCF-7 and MDA-MB-231), lung (A-549), prostate (PC-3) and cervix (HeLa and C33-A) cancer cell lines. Cell viability assays were conducted in quadruplicates and the half-maximal inhibitory concentration (IC_{50}) was calculated from the dose response diagrams (**Figure S13).** The IC_{50} for MCF-7, MDA-MB-231, A-549, PC-3, C33-A and HeLa cells was found to be reduced for NCND-PTX as compared to the free drug (**Table 1**). The cytotoxicity of NCND-PTX can be attributed to the release of free PTX molecules from the conjugate since the NCNDs do not induce any cytotoxic effect. Moreover, the data show that the conjugation of PTX to the dots affects the activity of the drug resulting in a higher anti-proliferative effect on the majority of the studied cells. The proliferation of MCF-7, MDA-MB-231, A-549, PC-3 and C33-A cancer cells was more inhibited with NCND-PTX treatment as compared to PTX treatment, while only the inhibition of the proliferation of HeLa cells after exposure to the conjugate was comparable with the PTX alone. The beneficial effect observed for the conjugate could be related to an improved biovailability of the drug, as a result of an enhanced aqueous solubility, a size that does not inhibit the entry of the drug into the cells and does not affect the mechanism of internalization, and a linker that allows the release of the drug from the conjugate.[48]

Finally, statistical analyses for each cell lines incubated with different NCND-PTX concentrations (from 0.02 to 2 μg·mL^{-1}) were carried out. As reported in **Figure S14**, the conjugate concentration has effect on the cell viability. For instance, a treatment with an increase of the NCND-PTX concentration from 0.25 to 0.4 μg·mL^{-1} resulted in the two times decrease of the C33-A cell viability (**Figure 5**).

3.4 Real-time monitoring of cell viability

The biological response of the NCND-PTX hybrid was further evaluated by using the xCELLigence system.[46,57] This has

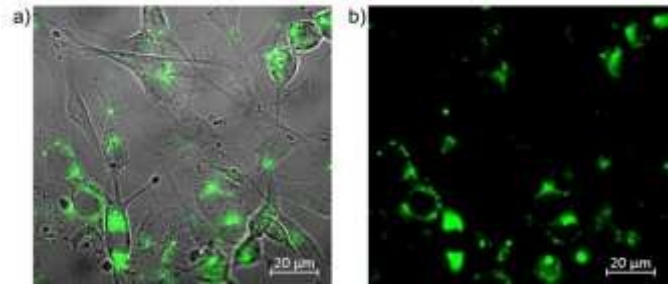

Figure 4. Confocal fluorescence images of C33-A cells after incubation with 300 μg·mL^{-1} NCNDs: **a)** Merged picture of the fluorescent bright field; **b)** fluorescent image.

proven to be a valuable tool for providing data about the global cell activities that cannot be acquired from the conventional tetrazolium-based viability single end-point assays. The system allows label-free and dynamic monitoring of cellular phenotypic changes, such as cell number, proliferation and growth, size and morphology. Therefore, xCELLigence provides a multi-parametric biological analysis in real time. It is based on electrical impedance measurements across interdigitated micro-electrodes integrated on the bottom of cell culture plates that are displayed as Cell Index (CI) values. CI values are defined as relative changes in electrical impedance created by attached cells and provide information about the biological status of the cells measuring cell adhesion within the well. For instance, if cells detach and die during cytotoxic events the cell-covered area reduces and CI values decrease. Moreover, continuous monitoring of cellular responses to biologically active compounds produces time-dependent cellular response profiles (TCRPs) that are characteristic for each agent. Therefore, impedance-based technology can be predictive of the biological activity and may be useful for determining the mode and mechanism of interaction.[46]

PTX is a powerful anti-mitotic agent that acts by promoting tubulin assembly into stable aggregated structures, inhibiting the normal dynamics reorganization of the microtubules, which results in mitotic arrest. We used the xCELLigence system to monitor the entire course of NCND-PTX interaction with cancer cells and gain insight into the mechanism of action of the drug. Impedance-based TCRPs reflect global cellular morphological responses to antimitotic agents and represent a unique signature for mitotic arrest. It has been reported that the exposure of different cell types to paclitaxel results in overall similar TCRPs profile.[46] Therefore, we selected A549 cells as model cell line for the study. **Figure 6** shows the TCRPs obtained when A549 cells were treated with different concentrations of NCND-PTX. The curves showed a dose dependent cell response to the conjugate. CI values shows that

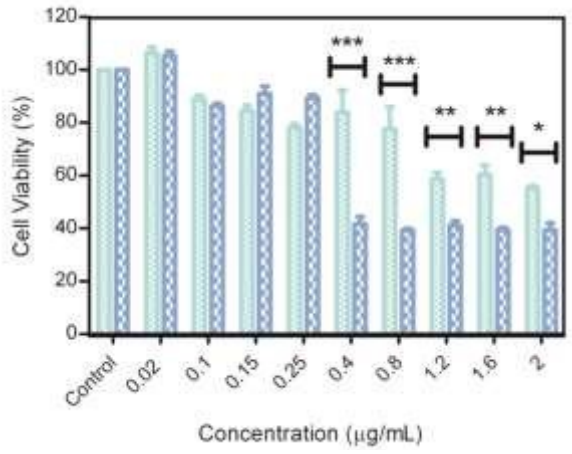

Figure 5. Cell viability of NCND-PTX and PTX in C33-A cancer cell line at 72 h of incubation. Cells were treated with PTX (green bars) and NCND-PTX (blue bars). The statistical analyses were performed using two-way ANOVA followed by Bonferroni's test. Data are expressed as mean ± SD (n=4). ***P < 0.001, **P < 0.01 and *P < 0.05.

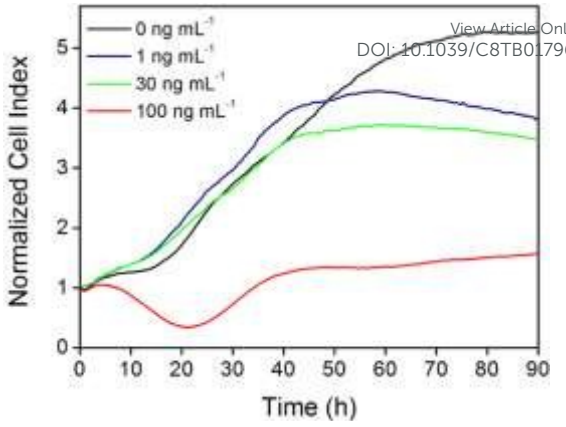

Figure 6. Normalized Cell Index kinetics of the A-549 cancer cells exposed to different concentrations of NCND-PTX.

following 20 h-incubation the highest concentration of NCND-PTX (100 ng·mL^{-1}) had significant anti-proliferative effects. The initial decline in cell index correlates with morphological changes due to cell rounding that result from mitotic arrest. Therefore, the conjugate induces significant cell death, as indicated by the rapid loss in the CI, and at the lowest point the majority of the cells are arrested. The observed kinetic profile resembled the one of the free PTX thus supporting the conclusion that the conjugate induced cell cycle arrest with the same mechanism of action observed for the free drug.

3.5 Apoptosis induced by CND-PTX

Confocal imaging along with nuclear fluorescence stain was used to probe the intracellular uptake and the effect on cellular nuclei. PTX is a microtubule-acting compound that affects the nuclear morphology inducing a nuclear fragmentation characteristic of apoptotic cell death.[58] Apoptotic cells lose substrate attachment and become rounded. To study if the conjugation of PTX with NCNDs modifies the apoptosis induced by the drug, the apoptosis was identified morphologically by 4',6-diamidino-2-phenylindole (DAPI) staining of DNA. Since the emission from DAPI and NCNDs overlapped, the latter were labelled with a cyanine dye (Cy5) (**Figures S4, S7-9**). The nuclei of A-549 cells treated with NCND-Cy5 (**Figure 7a**) showed homogeneous fluorescence with no evidence of condensation, fragmentation of the nuclei nor apoptotic bodies, which are typical features of cellular apoptosis.[59] In contrast, exposure of the cells to the conjugate, at a concentration of 20 ng·mL^{-1} (related to PTX), led to the characteristic apoptotic morphology with a grape shaped periphery and surrounding protrusions of chromatin, distributed in a few spherical apoptotic bodies (**Figure 7b**).[60] This result indicates that NCNDs do not affect the mechanism of action of PTX compared to the drug alone.

3.6 Drug release study

The similar mechanism of action and apoptosis-inducing effect of PTX and NCND-PTX suggests that the conjugate is functioning in a similar manner as the free drug, which can be ascribed to its release from the NCND carrier. Our linker design

is based on the hypothesis that the ester bond between the drug and the nanoparticles can be hydrolytically and/or enzymatically cleaved after cell internalization to release the cytotoxic agent. Since the 2'-hydroxyl group of the PTX is required for tubulin binding, the conjugate is anticipated to be

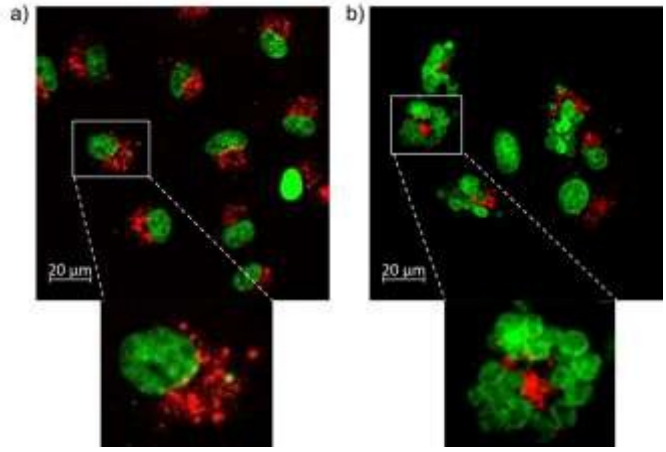

Figure 7. Apoptosis detection by confocal imaging of DAPI-nuclear stained (green), and NCND-Cy5 (red). A-549 cells treated with **a)** NCND-Cy5 and **b)** NCND-PTX- Cy5.

inactive unless internalized and hydrolyzed.[61]

The intracellular release of PTX from the conjugate was studied in the acute monocytic leukemia THP-1 cells that grow in suspension and have a high uptake rate. They were incubated with NCND-PTX for 24 h, then washed with media to remove the dots not attached to the cells and finally cell lysis was performed. Once the membrane-containing fraction was discharged, the presence of free NCNDs was observed in the water soluble fraction by fluorescence spectroscopy suggesting the release of the PTX from the dots (**Figure S10**).

Conclusions

In summary, we have reported a NCND-PTX drug delivery system based on a simple and effective covalent conjugation protocol. The conjugate provides an enhanced anticancer activity as compared to the free drug. Confocal microscopy confirmed the efficient cellular uptake of NCND-PTX and the apoptosis induced on cancer cells. Furthermore, the real-time monitoring of cell viability gave useful insights on the mechanism of action of the drug in the conjugate. The above results demonstrate the nanodot potential as vehicle for intracellular imaging and delivery of low water-soluble anticancer drugs.

Conflicts of interest

The authors declare no conflicts of interests.

Acknowledgements

MP, as the recipient of the AXA Chair, is grateful to the AXA Research Fund for financial support. MP was also supported by the Spanish Ministry of Economy and Competitiveness MINECO (project CTQ2016-76721-R), by the University of Trieste and by Diputación Foral de Gipuzkoa program Red (101). The authors thank Dr. Luka Đorđević for the help with NMR experiments and Dr. Sonia Serna with MALDI measurements.

References

1 Y.-P. Sun, B. Zhou, Y. Lin, W. Wang, K. A. S. Fernando, P. Pathak, M. J. Meziani, B. A. Harruff, X. Wang, H. Wang, P. G. Luo, H. Yang, M. E. Kose, B. Chen, L. M. Veca and S.-Y. Xie, *J. Am. Chem. Soc.*, 2006, **128**, 7756–7757.

2 S. N. Baker and G. A. Baker, *Angew. Chem. Int. Ed.*, 2010, **49**, 6726–6744.

3 S. Y. Lim, W. Shen and Z. Gao, *Chem. Soc. Rev.*, 2015, **44**, 362–381.

4 Y. Choi, Y. Choi, O.-H. Kwon and B.-S. Kim, *Chem. - An Asian J.*, , DOI:10.1002/asia.201701736.

5 H. Feng and Z. Qian, *Chem. Rec.*, 2018, **18**, 491–505.

6 Z. Qian, J. Ma, X. Shan, H. Feng and L. Shao, *Chem. - Eur. J.*, 2014, **20**, 2254–2263.

7 X. Li, M. Rui, J. Song, Z. Shen and H. Zeng, *Adv. Funct. Mater.*, 2015, **25**, 4929–4947.

8 F. Yuan, S. Li, Z. Fan, X. Meng, L. Fan and S. Yang, *Nano Today*, 2016, **11**, 565–586.

9 G. E. LeCroy, S.-T. Yang, F. Yang, Y. Liu, K. A. S. Fernando, C. E. Bunker, Y. Hu, P. G. Luo and Y.-P. Sun, *Coord. Chem. Rev.*, 2016, **320**–**321**, 66–81.

10 Y. Park, J. Yoo, B. Lim, W. Kwon and S.-W. Rhee, *J. Mater. Chem. A*, 2016, **4**, 11582–11603.

11 F. Arcudi, L. Đorđević and M. Prato, *Angew. Chem. Int. Ed.*, 2017, **56**, 4170–4173.

12 S. Carrara, F. Arcudi, M. Prato and L. De Cola, *Angew. Chem. Int. Ed.*, 2017, **56**, 4757–4761.

13 F. Arcudi, V. Strauss, L. Đorđević, A. Cadranel, D. M. Guldi and M. Prato, *Angew. Chem. Int. Ed.*, 2017, **56**, 12097–12101.

14 A. Cadranel, V. Strauss, J. T. Margraf, K. A. Winterfeld, C. Vogl, L. Đorđević, F. Arcudi, H. Hoelzel, N. Jux, M. Prato and D. M. Guldi, *J. Am. Chem. Soc.*, 2018, **140**, 904–907.

15 F. Rigodanza, L. Đorđević, F. Arcudi and M. Prato, *Angew. Chem. Int. Ed.*, 2018, **57**, 5062–5067.

16 G. Chen, H. Feng, X. Jiang, J. Xu, S. Pan and Z. Qian, *Anal. Chem.*, 2018, **90**, 1643–1651.

17 H. Ao, H. Feng, X. Huang, M. Zhao and Z. Qian, *J. Mater. Chem. C*, 2017, **5**, 2826–2832.

18 C. Tang, J. Zhou, Z. Qian, Y. Ma, Y. Huang and H. Feng, *J. Mater. Chem. B*, 2017, **5**, 1971–1979.

19 L. Chai, J. Zhou, H. Feng, C. Tang, Y. Huang and Z. Qian, *ACS Appl. Mater. Interfaces*, 2015, **7**, 23564–23574.

20 K. Dimos, F. Arcudi, A. Kouloumpis, I. B. Koutselas, P. Rudolf, D. Gournis and M. Prato, *Nanoscale*, 2017, **9**, 10256–10262.

21 C. Rizzo, F. Arcudi, L. Đorđević, N. T. Dintcheva, R. Noto, F. D'Anna and M. Prato, *ACS Nano*, 2018, **12**, 1296–1305.

22 H. Zhao, J. Duan, Y. Xiao, G. Tang, C. Wu, Y. Zhang, Z. Liu and W. Xue, *Chem. Mater.*, 2018, **30**, 3438–3453.

23 J. Wang, X. Zhang, J. Wu, H. Chen, S. Sun, J. Bao, S. Li and H. Bi, *Nanoscale*, 2017, **9**, 15873–15882.

24 W. Li, H. Zhang, Y. Zheng, S. Chen, Y. Liu, J. Zhuang, W.-R.

Liu and B. Lei, *Nanoscale*, 2017, **9**, 12976–12983.
25 U. Baruah, A. Konwar and D. Chowdhury, *Nanoscale*, 2016, **8**, 8542–8546.
26 Z. Xie, F. Wang and C. Liu, *Adv. Mater.*, 2012, **24**, 1716–21.
27 N. L. Teradal and R. Jelinek, *Adv. Healthc. Mater.*, 2017, **1700574**, 1–36.
28 Z. Peng, X. Han, S. Li, A. O. Al-Youbi, A. S. Bashammakh, M. S. El-Shahawi and R. M. Leblanc, *Coord. Chem. Rev.*, 2017, **343**, 256–277.
29 J. Zhang and S. H. Yu, *Mater. Today*, 2016, **19**, 382–393.
30 P. G. Luo, S. Sahu, S.-T. Yang, S. K. Sonkar, J. Wang, H. Wang, G. E. LeCroy, L. Cao and Y.-P. Sun, *J. Mater. Chem. B*, 2013, **1**, 2116–2127.
31 Z. Liu, X. Chen, X. Zhang, J. J. Gooding and Y. Zhou, *Adv. Healthc. Mater.*, 2016, **5**, 1401–1407.
32 T. Feng, X. Ai, G. An, P. Yang and Y. Zhao, *ACS Nano*, 2016, **10**, 4410–4420.
33 Z. Peng, E. H. Miyanji, Y. Zhou, J. Pardo, S. D. Hettiarachchi, S. Li, P. L. Blackwelder, I. Skromne and R. M. Leblanc, *Nanoscale*, 2017, **9**, 17533–17543.
34 X. Gong, Q. Zhang, Y. Gao, S. Shuang, M. M. F. Choi and C. Dong, *ACS Appl. Mater. Interfaces*, 2016, **8**, 11288–11297.
35 H.-J. Wang, X. He, T.-Y. Luo, J. Zhang, Y.-H. Liu and X.-Q. Yu, *Nanoscale*, 2017, **9**, 5935–5947.
36 W.-Q. Li, Z. Wang, S. Hao, L. Sun, M. Nisic, G. Cheng, C. Zhu, Y. Wan, L. Ha and S.-Y. Zheng, *Nanoscale*, 2018, **10**, 3744–3752.
37 W. J. Slichenmyer and D. D. Von Hoff, *J. Clin. Pharmacol.*, 1990, **30**, 770–788.
38 M. A. Jordan and L. Wilson, *Nat. Rev. Cancer*, 2004, **4**, 253–65.
39 H. Gelderblom, J. Verweij, K. Nooter and A. Sparreboom, *Eur. J. Cancer*, 2001, **37**, 1590–8.
40 J. Szebeni, C. R. Alving and F. M. Muggia, *JNCI J. Natl. Cancer Inst.*, 1998, **90**, 300–306.
41 P. Ma and R. J. Mumper, *J Nanomed Nanotecghnology*, 2013, **4**, 1–35.
42 A. M. Sofias, M. Dunne, G. Storm and C. Allen, *Adv. Drug Deliv. Rev.*, 2017, **122**, 20–30.
43 F. Wang, M. Porter, A. Konstantopoulos, P. Zhang and H. Cui, *J. Control. Release*, 2017, **267**, 100–118.
44 H. M. Deutsch, J. A. Glinski, M. Hernandez, R. D. Haugwitz, V. L. Narayanan, M. Suffness and L. H. Zalkow, *J. Med. Chem.*, 1989, **32**, 788–792.
45 F. Arcudi, L. Đorđević and M. Prato, *Angew. Chem. Int. Ed.*, 2016, **55**, 2107–2112.
46 Y. A. Abassi, B. Xi, W. Zhang, P. Ye, S. L. Kirstein, M. R. Gaylord, S. C. Feinstein, X. Wang and X. Xu, *Chem. Biol.*, 2009, **16**, 712–723.
47 Q. Shi, H. Wang, K. F. Bastow, Y. Tachibana, K. Chen, F. Lee and K. Lee, *Bioorg. Med. Chem.*, 2001, **9**, 2999–3004.
48 J. J. Khandare, S. Jayant, A. Singh, P. Chandna, Y. Wang, N. Vorsa and T. Minko, *Bioconjug. Chem.*, 2006, **17**, 1464–1472.
49 Y. Yang, H. Aloysius, D. Inoyama, Y. Chen and L. Hu, *Acta Pharm. Sin. B*, 2011, **1**, 143–159.
50 J. D. Gibson, B. P. Khanal and E. R. Zubarev, 2007, **129**, 11653–11661.
51 L. Đorđević, T. Marangoni, T. Miletic, J. Rubio-magnieto, J. Mohanraj, H. Amenitsch, D. Pasini, N. Liaros, S. Couris, N. Armaroli, M. Surin and D. Bonifazi, *J. Am. Chem. Soc.*, 2015, **137**, 8150–8160.
52 Y. Cohen, L. Avram and L. Frish, *Angew. Chem. Int. Ed.*, 2005, **44**, 520–554.
53 L. Wang, S. Zhu, H. Wang, S. Qu, Y.-L. Zhang, J. Zhang, Q. Chen, H.-L. Xu, W. Han, B. Yang and H.-B. Sun, *ACS Nano*, 2014, **8**, 2541–2547.
54 F. Ehrat, S. Bhattacharyya, J. Schneider, A. Löf, R. Wyrwich, A. L. Rogach, J. K. Stolarczyk, A. S. Urban and J. Feldmann, *Nano Lett.*, 2017, **17**, 7710–7716.
55 M. Fu, F. Ehrat, Y. Wang, K. Z. Milowska, C. Reckmeier, A. L. Rogach, J. K. Stolarczyk, A. S. Urban and J. Feldmann, *Nano Lett.*, 2015, **15**, 6030–6035.
56 A. B. Etame, C. A. Smith, W. C. W. Chan and J. T. Rutka, *Nanomedicine Nanotechnology, Biol. Med.*, 2011, **7**, 992–1000.
57 J. Martinez-Serra, A. Gutierrez, S. Muñoz-Capó, M. Navarro-Palou, T. Ros, J. C. Amat, B. Lopez, T. F. Marcus, L. Fueyo, A. G. Suquia, J. Gines, F. Rubio, R. Ramos and J. Besalduch, *Onco. Targets. Ther.*, 2014, **7**, 985–94.
58 T. Wang and D. Ph, .
59 A. H. Wyllie, *Nature*, 1980, 284, 555–556.
60 M. Kihlmark, G. Imreh and E. Hallberg, *J. Cell Sci.*, 2001, **114**, 3643–3653.
61 K. C. Nicolaou, W.-M. Dai and R. K. Guy, *Angew. Chemie Int. Ed. English*, 1994, **33**, 15–44.

View Article Online
DOI: 10.1039/C8TB01796D

View Article Online
DOI: 10.1039/C8TB01796D

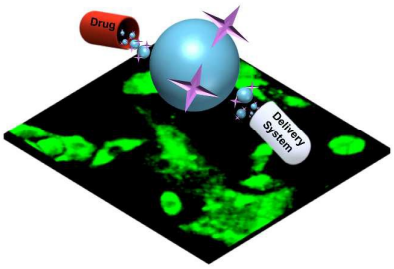

A carbon nanodots-paclitaxel drug delivery system with an enhanced anticancer activity as compared to the free drug is reported.